

Investigating the Role of Electric Fields on Flow Harmonics in Heavy-Ion Collisions

Ankit Kumar Panda,^{*} Reghukrishnan Gangadharan,[†] and Victor Roy[‡]
*School of Physical Sciences, National Institute of Science Education and Research,
An OCC of Homi Bhabha National Institute, Jatni-752050, India*

(Dated: January 3, 2023)

Using the blast-wave model, we explore the effect of electric fields on spectra and flow harmonics (especially the elliptic flow) for charged pions and protons. We incorporate the first-order correction to the single-particle distribution function due to the electric fields and the dissipative effect while calculating the invariant yields of hadron in the Cooper-Frey prescription at the freezeout hypersurface. We find a noticeable correction to the directed and elliptic flow of pions and protons for unidirectional and azimuthal asymmetric electric fields in the transverse plane of magnitude $\sim m_\pi^2$. Further, we observe mass dependency of the directed flow generated due to the electric fields. The splitting of particle and antiparticle's elliptic flow is also discussed.

I. INTRODUCTION

In high energy heavy-ion collisions at RHIC and LHC, two highly Lorentz contracted nuclei colliding onto one another produces a hot and dense novel state of matter known as Quark Gluon Plasma (QGP). The QGP formed in heavy-ion collisions is the same as the medium that existed during the microsecond old universe, which consisted of almost freely moving quarks and gluons that are usually confined in colorless hadrons at low or zero temperatures [1, 2]. Hydrodynamic calculations have confirmed that the QGP is a strongly coupled fluid with extremely low $\frac{\eta}{s}$ value [3–5]. Along with the QGP, an intense electromagnetic field of the order of 10^{14} T is generated in the initial stage of heavy ion collision in Au+Au collision at top RHIC energies [6–12]. The primary source of intense electromagnetic (EM) fields in heavy-ion collisions are the spectator nucleons (the nucleons that are unaffected by collisions).

Relativistic viscous hydrodynamics is a well-established formalism for describing the space-time evolution of the quark-gluon plasma (QGP). However, owing to the finite electrical conductivity of the high temperature QGP and low temperature hadronic gas phase both phases evolving in intense EM fields, the proper framework, we believe, is the relativistic resistive magnetohydrodynamics (RRMHD). The straightforward generalization of non-relativistic viscous hydrodynamics to the relativistic regime leads to an acausal theory. The acausality problem is usually cured by incorporating higher-order gradient terms in the entropy-four current or in the energy-momentum tensor of the fluid [13]. The space-time evolution of the QGP should be studied using a causal RRMHD theory. There have been recent developments on the formulation of causal (second-order) magnetohydrodynamic formalisms from the kinetic theory perspective [14–19]. Most of these

studies have reported a few new transport coefficients arising due to the external EM fields, some of which were non-dissipative as they did not increase entropy. However, a systematic investigation of many of these transport coefficients has not yet been done. Moreover, the effect of electric fields on bulk observables such as transverse momentum (p_T) spectra and flow coefficients of charged hadrons has not been extensively studied, to our knowledge, except for a few studies [20, 21]. Developing a RRMHD numerical code is a challenging task [22, 23], and it is known that viscosity (and EM fields) affects the space-time evolution of the fluid and also the one-particle thermal distribution of particles used in the Cooper-Frye formulation, which ultimately gives the final experimentally observed particles from the fluid elements.

Here, we use a simple but effective blastwave model [24] to investigate the influence of the electric field on experimental bulk observables such as first and second-order flow harmonics (v_1, v_2) and transverse momentum (p_T) spectra of charged hadrons, due to corrections only in the Cooper-Frye prescription. These observables are known as ‘bulk observables’ because they involve the collective motion of many particles in the fluid. The effect of viscous corrections is introduced through a relaxation time τ_c , which is a free parameter in our case. We note that a more accurate estimate of the effect of EM fields on bulk observables requires a magnetohydrodynamic evolution [22] of the fluid. It is important to note that in addition to second-order flow harmonics (v_2) and transverse momentum (p_T) spectra of charged hadrons, the electromagnetic field may result in a variety of other novel phenomena such as the Chiral Magnetic Effect and Chiral Separation Effect [25–27]. Other works that study the effect of EM fields on the QGP include [28–32].

The article is organized as follows: we discuss the blast wave model in Section II, then we discuss the Cooper-Frye mechanism and other relevant formulas, along with the setup, in Sections III and IV. Results are discussed in Section V. Finally, we conclude and summarize our study in Section VI. Throughout the article, we use natural units where $\hbar = c = k_B = 1$. The metric signature used here is $g_{\mu\nu} = \text{diag}(+, -, -, -)$.

^{*} ankitkumar.panda@niser.ac.in

[†] reghukrishnang@niser.ac.in

[‡] victor@niser.ac.in

II. BLAST WAVE MODEL

The blast-wave model is a simple model that considers the collective motion of the matter produced in heavy-ion collisions and parameterizes its four-velocity. It further assumes that hadrons are produced from a constant temperature freeze-out hypersurface, with the freeze-out temperature being a free parameter. The invariant yields of hadrons are obtained from the Cooper-Frye formalism, which is described later. Despite its simplicity, the blast-wave model can successfully describe experimental data qualitatively and quantitatively in most cases.

In heavy-ion collisions, one popular parametrization of the fluid four-velocity is inspired by the Bjorken model of boost-invariant expansion in the longitudinal direction of the fluid. In this work, we use the Milne coordinate (τ, η, r, ϕ) with the metric $g_{\mu\nu} = \text{diag}(1, -\tau^2, -1, -r^2)$, and the transformation between the Cartesian and Milne coordinate is given as

$$\begin{bmatrix} t \\ x \\ y \\ z \end{bmatrix} = \begin{bmatrix} \cosh\eta & 0 & 0 & 0 \\ 0 & 0 & \cos\phi & 0 \\ 0 & 0 & \sin\phi & 0 \\ \sinh\eta & 0 & 0 & 0 \end{bmatrix} \begin{bmatrix} \tau \\ \eta \\ r \\ \phi \end{bmatrix}.$$

Where

$$\begin{aligned} \tau &= \sqrt{t^2 - z^2}, \\ \eta &= \tanh^{-1} z/t, \\ r &= \sqrt{x^2 + y^2}, \\ \phi &= \arctan 2(y, x). \end{aligned}$$

The parameterized form of the velocity four vector with longitudinal boost-invariance is given as

$$\begin{aligned} u^r &= u_0 \frac{r}{R} \left[1 + 2 \sum_{n=1}^{\infty} c_n \cos n[\phi - \psi_n] \right] \Theta(R - r), \\ u^\phi &= u^\eta = 0, \\ u^\tau &= \sqrt{1 + (u^r)^2}. \end{aligned} \quad (1)$$

Where, $u^\tau, u^r, u^\phi, u^\eta$ are the components of the fluid four velocity; u_0 , and c_n 's are free parameters used to reproduce the p_T spectra (invariant yield) and the flow harmonics of charged hadrons. $\Theta(R - r)$ is the Heaviside function which imposes the condition that if $r > R$, $u^r = 0$. R is the radius of the freezeout hypersurface, ϕ is the azimuthal angle in co-ordinate space and ψ_n is the n -th order participant plane angle. As we do not consider event-by-event fluctuations in this work, we set $\psi_n = 0$ i.e., the minor axis of the participant planes coincide with the direction of the impact parameter. We parametrised the temperature on the freezeout hypersurface as

$$T(\tau, \eta, r, \phi) = T_0 \Theta(R - r).$$

Where T_0 denotes the temperature at the freezeout hypersurface.

III. COOPER-FREY FORMALISM

As mentioned earlier, the invariant yield of hadrons is obtained from the Cooper-Frye formula [33], which assumes that the freeze-out hypersurface is a timelike vector $d\Sigma_\mu$ given by $(\tau d\eta dr r d\phi, 0, 0, 0)$. The invariant yield is given by the following equation:

$$\frac{dN}{d^2 p_T dy} = \frac{\mathcal{G}}{(2\pi)^3} \int p^\mu d\Sigma_\mu f(x, p). \quad (2)$$

Here, $f(x, p)$ is the single-particle distribution function, and x and p are the position and momentum four-vectors of the particles, respectively. \mathcal{G} is the degeneracy factor.

If the system is not in local thermal equilibrium, as is the case for a rapidly expanding fireball, the single-particle distribution function must take into account the deviation from equilibrium when calculating hadron yields using the Cooper-Frye prescription. The distribution function is usually decomposed into an equilibrium part f_0 and a small non-equilibrium part δf , so that the total distribution function becomes $f = f_0 + \delta f$. The second-order correction to f gives rise to some new transport coefficients due to the external magnetic field. The temperature and mass dependence of some of these transport coefficients were discussed in [34], and we will show the results for the remaining coefficients later in the Results section.

However, in this work, we consider terms up to first-order in gradients [17]. In this case, the invariant yield (Eq. (2)) becomes

$$\frac{dN}{d^2 p_T dy} = \frac{\mathcal{G}}{(2\pi)^3} \int p^\mu d\Sigma_\mu (f_0 + \delta f^1). \quad (3)$$

Where $\delta f^1 \ll f_0$. In [16, 17] δf^1 is calculated using the Boltzmann equation using the Relaxation Time Approximation (RTA). We give the expression for δf^1 in Appendix.(B) for the sake of completeness.

IV. SETUP

For the current study, we consider only $n = 2$ in the expression for u^r (Eq.(1)), resulting in

$$u^r = u_0 \frac{r}{R} [1 + 2c_2 \cos(2\phi)] \Theta(R - r).$$

The equilibrium distribution is $f_0 = (e^{\beta u \cdot p - \alpha} + r)^{-1}$, here β is the inverse temperature, $r = \pm 1$ corresponds to fermions and bosons respectively. We use the parameters given in Table (I) to obtain the invariant yield of π^+ that matches the ALICE measurement shown as red circles in the top panel of Fig.(1)[35]. Earlier hydrodynamic model studies [36] have shown that it is not possible to simultaneously describe π^+ and p spectra for zero baryon chemical potential, so we use a different set of values for u_0 , c_2 , and T (given in the rightmost column of

Table (I) to explain the proton spectra. The blast-wave model with these parameters reasonably well explains the experimental data. The bottom panel of Fig. (1) shows the blast-wave results for v_2 of π^+ and p. We do not compare these ideal results with experimental data since they are known to over-predict the experimental measurements, but we show them for the sake of qualitative description.

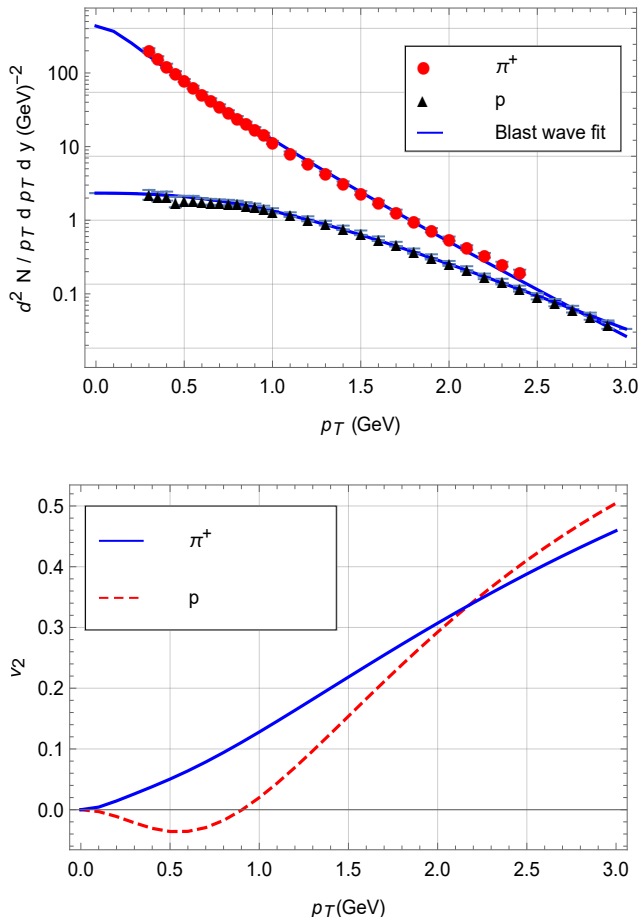


FIG. 1: (Color online) Top plot is the comparison of the experimentally measured π^+ (red filled circles) and protons (black triangles) for Pb+ Pb collision at $\sqrt{s}=2.76$ TeV for 20-30 % centrality with the ideal blast wave results (lines) for the parameters in Table (I). The lower panel shows the corresponding v_2 vs p_T for π^+ (blue line) and protons (red dashed line).

After setting up the parameters for the ideal case (zero viscosity), we can now explore the effect of viscosity (through the relaxation time τ_c) and electric fields on spectra and flow harmonics by comparing the corresponding results with the ideal results. In our model, τ_c and the electric field qE appear in δf^1 , giving rise to additional corrections to the invariant yields and flow harmonics of charged hadrons. We compute the p_T differ-

ential n -th order flow coefficient using the usual formula:

$$v_n(p_T, y) = \frac{\int_0^{2\pi} d\varphi \cos(n\varphi) \frac{dN}{d^2 p_T dy}}{\int_0^{2\pi} d\varphi \frac{dN}{d^2 p_T dy}}. \quad (4)$$

As we need the electric field distribution on the freeze-

	π^+	p
u_0	1.2	1.22
T	130 MeV	140 MeV
R	10 fm	10 fm
τ	6 fm	6 fm
m	139.5 MeV	938 MeV
c_2	0.1	0.15

TABLE I: The fit parameters for π^+ and p respectively at mid-rapidity.

out hypersurface to be used in the Cooper-Frye formula (Eq.(2)) we use a parameterized form of the EM field. In principle, the fields generated in the initial stages of heavy-ion collisions due to the charged protons inside the two colliding nucleus would evolve with the QGP fluid, but the blast wave model does not allow any such self-consistent dynamical evolution of fields. The magnitude of the electric fields in all the cases are kept Here we use parameterised electric fields of four different configurations in the transverse plane (XY plane) while calculating the invariant yields. Some of these configurations does not represent the actual scenario encountered in heavy-ion collisions but we use them for exploratory purpose. In the left panel of Fig.(2) we show the first setup of electric fields which we call **config-1** henceforth, this represents isotropic fields due to a point charge of large magnitude at the origin, the right panel shows **config-2** that closely resembles the field configuration expected in symmetric heavy-ion collision. **config-3** as shown in the left panel of Fig.(2) is the $\pi/2$ rotated version of **config-2**. The right panel of Fig.(2) represents a constant unidirectional electric fields which might be applied in a limited sense for large-small nuclei collisions, this is **config-4**. To better understand the effect of electric fields on flow harmonics we note the following

- **config-1**: isotropic fields; expected to unalter the flow harmonics,
- **config-2**: prolate-like fields; expected to decrease the flow harmonics,
- **config-3**: oblate-like fields; expected to increase the flow harmonics,
- **config-4**: directional fields; expected to alter directional flow only.

V. RESULTS

Here we discuss our main results for different configurations of electric fields (described in the previous section)

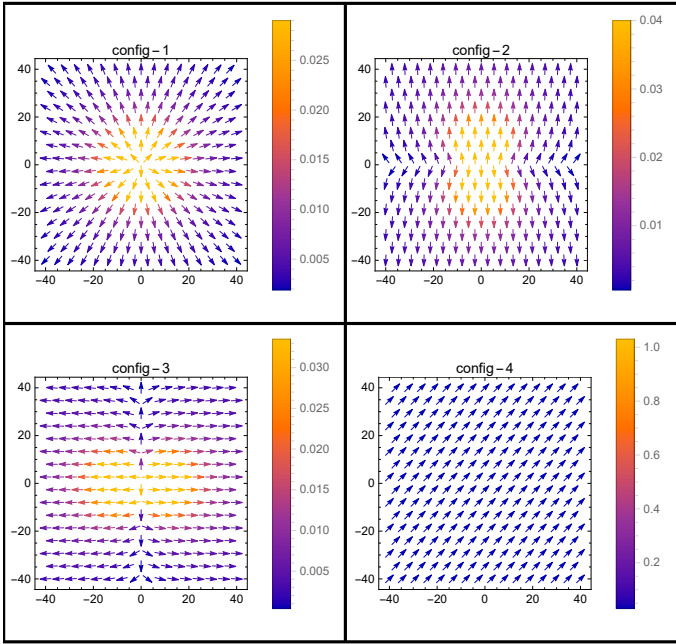


FIG. 2: (Color online) Electric field configurations in the transverse plane. Detail expressions for different configurations are given in Appendix.(B1). Magnitude of electric fields (in GeV^2) are shown using colour map.

on the spectra, and v_2 for pions and protons. Top panel of Fig.(3) shows the dependence of p_T spectra of π^+ on the electric fields for ideal case, for comparison we also show the results for non-zero viscosity but with no electric fields. The magnitude of viscosity in our model is controlled through t_c which is set to 1 fm for the results shown here. Here we see that the p_T spectra hardly shows any dependence on different transverse electric field configurations (solid orange, black, red lines correspond to **config-1**, **config-2**, and **config-3** respectively). As expected the effect of finite viscosity is comparatively more prominent on the p_T spectra; we see a suppression at higher p_T region for the viscous case. Since both bulk and shear viscosity is present in our case, the slope of the spectra is determined by the relative contributions of these two viscosities [37, 38]. The bottom panel of Fig.(3) shows the p_T spectra for protons for ideal (with electric fields) and viscous (without electric field) cases where we see a small suppression in the lower p_T region for the case of **config-2** and **config-3** for ideal case. We also see a suppression at higher p_T for viscous case as was seen for π^+ .

Before discussing the differential v_2 for different cases, it is worthwhile to explore the dependence of p_T integrated (0-3 GeV) $dN/d\phi$ on different field configurations and viscosity. In the top panel of Fig.(4) we show the $dN/d\phi$ of π^+ as a function of ϕ for various cases. As expected we have pure cosine like dependence of $dN/d\phi$ for ideal case (shown by the solid blue line), the viscosity re-

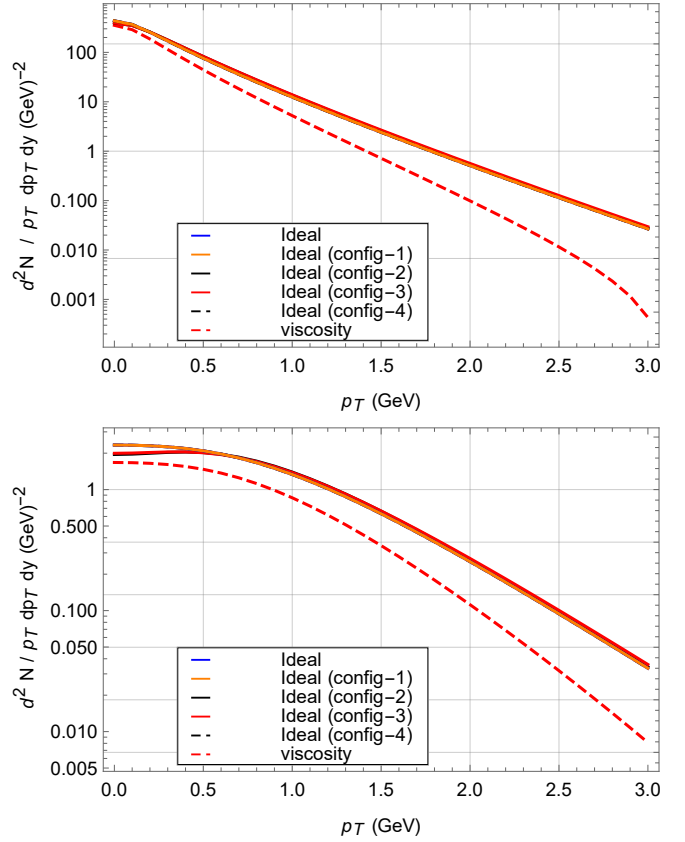


FIG. 3: (Color online) Upper panel represents the p_T Spectra for π^+ and lower panel for proton with different transverse field configurations as in Fig.(2) and for the case of viscosity for $t_c = 1\text{fm}$.

duces the multiplicity as well as the amplitude (shown by the red dashed line). **config-1** the isotropic field configuration (orange solid line) almost coincides with the ideal result, but we see noticeable change in the amplitude of $dN/d\phi$ for **config-2**, **config-3** as expected. Things become more interesting for **config-4** (black dashed line), here we generate finite directed flow like behaviour, this is understood from the fact that a unidirectional force shifts the centre of mass of the distribution. Similar behaviour was observed for protons also (shown in the bottom panel of Fig.(4)).

A more concrete way to study the angular dependence of $dN/d\phi$ for **config-4** can be achieved by using a finite Fourier series decomposition of $dN/d\phi$ as shown in Eq.(5).

$$f(\Phi) = N \left[1 + 2 \sum_{n=1}^3 v_n \cos(n\Phi) + 2 \sum_{n=1}^3 w_n \sin(n\Phi) \right]. \quad (5)$$

A non-linear least squares fit with v_n , w_n and N as a free-parameters we obtain the best fit for $dN/d\phi$ with the values of these parameters given in Table (II). Here we note that the directional force v_1 is larger than v_2 for π^+ , and

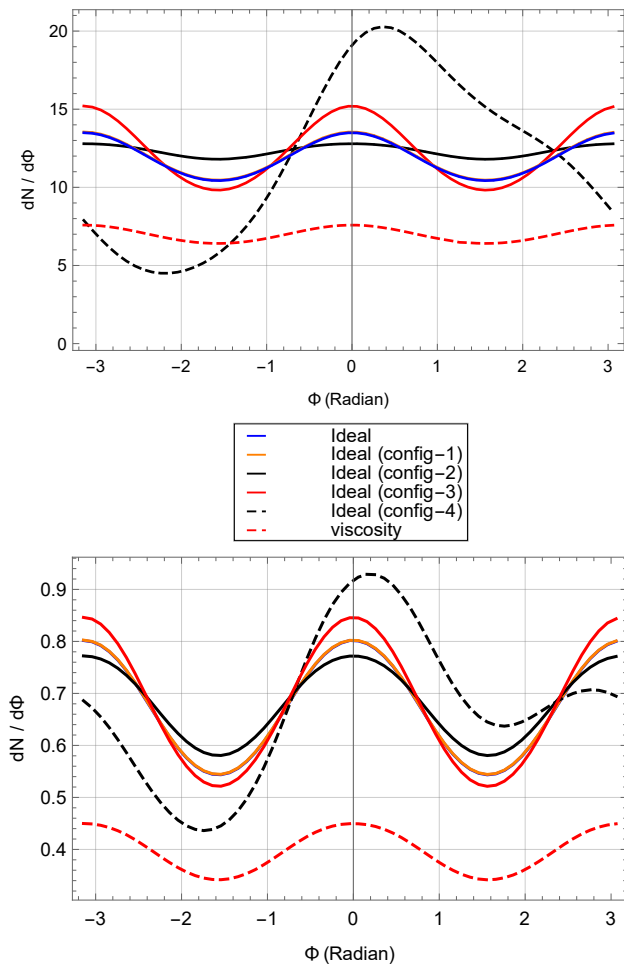


FIG. 4: (Color online) Top panel: $dN/d\phi$ as a function of ϕ for π^+ for various field configurations. Bottom panel: same as top panel but for proton.

they are similar in magnitude for protons. Moreover, we notice that unlike other cases the azimuthal distribution breaks reflection symmetry with respect to the Y axis which gives rise to non-zero w_n shown in Table (II). We also observe a mass dependence of the directional flow as π^+ has a larger v_1 compared to the protons.

	π^+	p
N	$11.907 \pm 2.7\text{e-}05$	$0.672 \pm 7.1\text{e-}08$
v_1	$0.218 \pm 1.0\text{e-}07$	$0.081 \pm 7.9\text{e-}08$
v_2	$0.064 \pm 9.8\text{e-}08$	$0.096 \pm 7.9\text{e-}08$
v_3	$0.017 \pm 9.7\text{e-}08$	$0.005 \pm 7.8\text{e-}08$
w_1	$0.213 \pm 1.0\text{e-}07$	$0.081 \pm 7.9\text{e-}08$
w_2	$0.000 \pm 9.8\text{e-}08$	$0.000 \pm 7.8\text{e-}08$
w_3	$0.017 \pm 9.8\text{e-}08$	$0.005 \pm 7.8\text{e-}08$

TABLE II: Fit parameters for π^+ and proton for **config-4** from Eq.(5).

To have a visual understanding of the goodness of fit, we show a comparison of the fitted values (using Eq.(5))

(solid blue line) and the $dN/d\phi$ from the blast wave model (dotted-dash orange line) for π^+ (top panel) and proton (bottom panel) in Fig.(5).

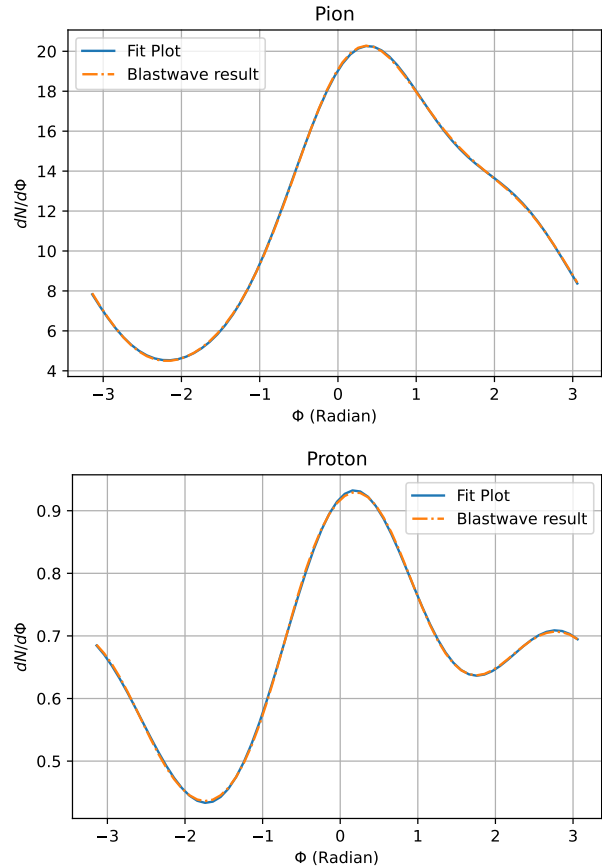


FIG. 5: (Color online) Blast wave results and the fitted curves using Eq.(5) for **config-4** for π^+ (top panel) and proton (bottom panel).

More familiar and useful observables in experiments are centrality and p_T dependent flow harmonics. In Fig.(6) we show the dependence of the second-order flow harmonics v_2 (a.k.a elliptic flow) for different configurations. Here we see that there is almost no deviation from the ideal case for the isotropic (**config-1**) and directed field case (**config-4**). However, the situation is different for the other two cases, we can clearly see an increase in v_2 for **config-3** and a suppression for **config-2**. We also note that viscosity suppresses the elliptic (red dashed line) flow for π^+ and elevates for proton.

The effect of electric fields become more interesting when we examine the difference in v_2 for particles (π^+ , p) and antiparticles (π^- , \bar{p}). This difference $\Delta v_2 = v_2(h) - v_2(\bar{h})$ is shown in Fig.(7) as a function of p_T . We observe a non-monotonic variation in Δv_2 as a function of p_T for both pions and protons. Interestingly, a similar observation was made in [29].

Throughout this study we only consider the effect of

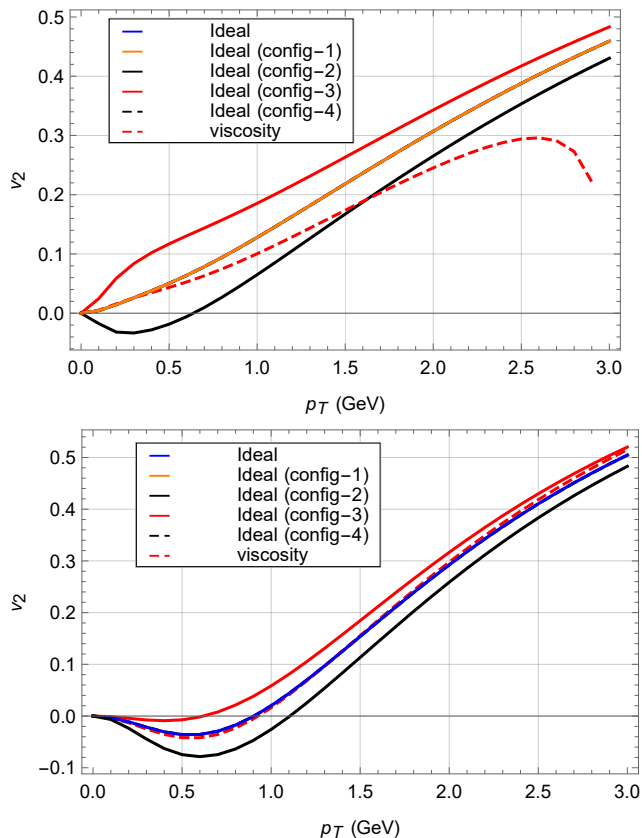


FIG. 6: (Color online) v_2 vs p_T for π^+ (top panel) and proton (bottom panel) for the transverse electric field configurations shown in Fig.(2).

electric fields and the first order correction in the δf . As mentioned earlier, previous studies showed that there are new transport coefficients at higher order corrections to f which may alter the results obtained here. But these are beyond the scope of the present exploratory study. In Fig.(8) we show the temperature and mass dependence of some of the transport coefficients arising due to the magnetic fields. This may give some hints of the relative contribution of various transport coefficients in the bulk observables while used in the Cooper-Frye prescription.

VI. SUMMARY AND CONCLUSION

In this work, we have studied the effect of electric fields on the bulk observables in heavy-ion collisions such as p_T spectra, directed and elliptic flow of charged pions and protons. We use the blast-wave model and different configurations of electric fields in the transverse plane to carry out this exploratory study. The p_T spectra of hadrons in the blast-wave model are obtained using Cooper-Frye prescription, where we incorporate non-equilibrium correction δf due to the viscosity and the electric fields. Since the blast-wave model does not in-

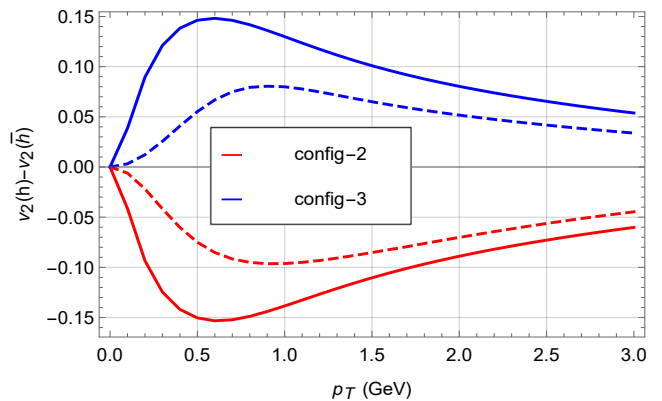


FIG. 7: (Color online) $v_2(h) - v_2(\bar{h})$ as a function of p_T for **config-2** (red) and **config-3** (blue) line corresponds to π (Solid line) and p (Dashed line).

clude space-time evolution, the fluid velocity and the electric fields are parameterized on the freezeout hypersurface to calculate experimental observables. For our case, fluid velocity fields are modulated so that it dominantly generates the elliptic flow. We use four different configurations of transverse electric fields (i) isotropic fields, (ii) prolate-like fields, (iii) oblate-like fields, and (iv) directed fields. The typical maximum value of the electric field for all these configurations is $\sim m_\pi^2$. We find that flow harmonics for isotropic fields remain unchanged for both pions and protons. Both prolate and oblate-like field configuration alters the flow harmonics, and the directed field gives rise to large directed flow v_1 for both pions and protons. We also observe a mass dependence of v_1 generated due to the electric fields. We also discuss the temperature and mass dependence of some of the new transport coefficients that appear in the second-order correction in the distribution function due to the EM field. They can further contribute to the results we obtained here. This we leave for a possible future study.

ACKNOWLEDGMENTS

AP acknowledges the CSIR-HRDG financial support. RG and VR acknowledge support from the DAE, Govt. of India.

Appendix A: Appendix

In this work we have used Milne coordinate system (τ, η, r, ϕ) , where $\tau = \sqrt{t^2 - z^2}$, $r = \sqrt{x^2 + y^2}$, $\eta = \tanh^{-1}(z/t)$, and $\phi = \tan^{-1}(y/x)$, due to the co-ordinate transformation various equations changed forms compared to the Cartesian coordinates. Here we give the details about the Jacobian and Christoffel symbols used in this study due to the above coordinate transformation:

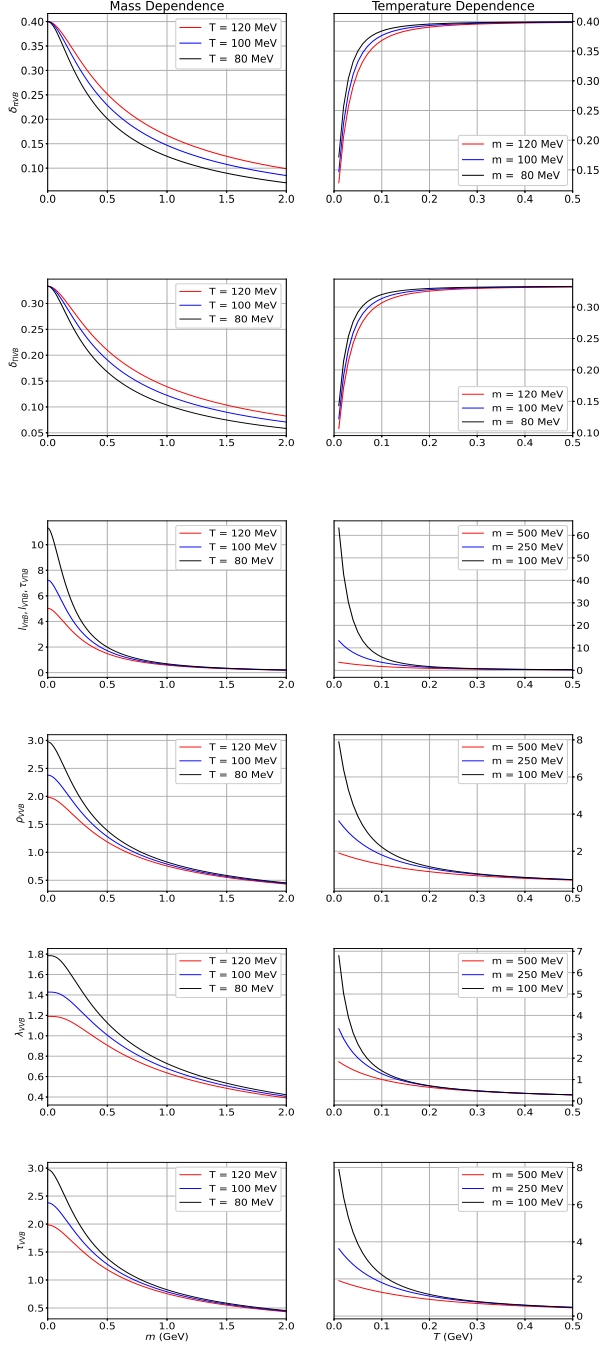


FIG. 8: (Color online) Mass and temperature variation of the transport coefficients arising due to external magnetic field.

Appendix B: First-order (δf) correction to the single-particle distribution

In Eq.(3) we introduced the first-order correction to the single-particle distribution while calculating invariant yield using the Cooper-Frye formula. Here we give the detail expression of δf in terms of gradients of fluid variables and

the Jacobian for volume element is $\sqrt{-g} = \tau r$ and the non-vanishing Christoffel symbols are $\Gamma_{\eta\eta}^r = \tau, \Gamma_{\tau\eta}^\eta = \frac{1}{\tau}, \Gamma_{\phi\phi}^r = -r, \Gamma_{r\phi}^\phi = \frac{1}{r}$. The space-like projection is defined as $\Delta^{\mu\nu} = g^{\mu\nu} - u^\mu u^\nu$; for Milne coordinate system, different components of $\Delta^{\mu\nu}$ are $\Delta^{\tau\tau} = -(u^r)^2, \Delta^{\eta\eta} = -\frac{1}{\tau^2}, \Delta^{rr} = -1 - (u^r)^2, \Delta^{\phi\phi} = -\frac{1}{r^2}, \Delta^{\tau\eta} = \Delta^{\tau\phi} = \Delta^{\eta r} = \Delta^{\eta\phi} = \Delta^{r\phi} = 0, \Delta^{\tau r} = -\sqrt{1 + (u^r)^2} u^r$. The expansion scalar is given by $\theta = D_\mu u^\mu = \partial_\mu u^\mu + \Gamma_{\mu\alpha}^\mu u^\alpha$.

We consider real particles and the on-shell condition is given by $g_{\mu\nu} p^\mu p^\nu = (p^\tau)^2 - \tau^2 (p^\eta)^2 - (p^r)^2 - r^2 (p^\phi)^2 = m^2$. Following the convention used in heavy-ion collisions we express the components of the four momentum p^μ as $(E, p^x, p^y, p^z) = (m_T \cosh y, p_T \cos \varphi, p_T \sin \varphi, m_T \sinh y)$. Where $p_T = \sqrt{p_x^2 + p_y^2}$, $m_T = \sqrt{m^2 + p_T^2}$, and $y = \tanh^{-1}(p_z/E)$. The components of the four-momentum in Milne coordinates are

$$\begin{aligned} p^\tau &= m_T \cosh(y - \eta), \\ \tau p^\eta &= m_T \sinh(y - \eta), \\ p^r &= p_T \cos(\varphi - \phi), \\ r p^\phi &= p_T \sin(\varphi - \phi). \end{aligned}$$

φ is the azimuthal angle of the particle in the momentum space.

In Eq.(2) we have the term $p^\mu d\Sigma_\mu$ which in our is given by $p^\mu d\Sigma_\mu = g_{\mu\nu} p^\mu d\Sigma^\nu = m_T \cosh(y - \eta) \tau d\eta r dr d\phi$.

fields:

$$\begin{aligned}
\delta f &= -\frac{\tau_c}{u.p} \left(p^\mu \partial_\mu f_0 + q F^{\mu\nu} p_\nu \frac{\partial f_0}{\partial p^\mu} \right) \\
&= -\frac{\tau_c}{u.p} \left(-p^\mu f_0 \tilde{f}_0 [\beta p^\alpha D_\mu u_\alpha + (u.p) \partial_\mu \beta - \partial_\mu \alpha] \right) - \frac{\tau_c}{u.p} \left(-f_0 \tilde{f}_0 q F^{\mu\nu} p_\nu \beta \frac{\partial(u.p)}{\partial p^\mu} \right) \\
&= \frac{\tau_c f_0 \tilde{f}_0}{u.p} (\beta p^\mu p^\alpha D_\mu u_\alpha + (u.p) p^\mu \partial_\mu \beta - p^\mu \partial_\mu \alpha) - \frac{\tau_c f_0 \tilde{f}_0}{u.p} q \beta E^\nu p_\nu \\
&= \frac{\tau_c f_0 \tilde{f}_0}{u.p} \left(\beta p^\mu p^\alpha \left[u_\mu \dot{u}_\alpha + \sigma_{\mu\alpha} + \omega_{\mu\alpha} + \frac{\Delta_{\mu\alpha} \theta}{3} \right] + (u.p) p^\mu \partial_\mu \beta - p^\mu \partial_\mu \alpha \right) - \frac{\tau_c f_0 \tilde{f}_0}{u.p} q \beta E^\nu p_\nu \\
&= \frac{\tau_c f_0 \tilde{f}_0}{u.p} \left(\beta p^\mu p^\alpha \left[\sigma_{\mu\alpha} + \frac{\Delta_{\mu\alpha} \theta}{3} \right] + (u.p) p^\mu \partial_\mu \beta - p^\mu \partial_\mu \alpha \right) - \frac{\tau_c f_0 \tilde{f}_0}{u.p} q \beta E^\nu p_\nu \\
&= \frac{\tau_c f_0 \tilde{f}_0}{u.p} (\beta p^\mu p^\alpha \partial_\mu u_\alpha + \beta p^\phi p^\phi r u_r - \beta p^\eta p^\eta \tau u_\tau + (u.p) p^\mu \partial_\mu \beta - p^\mu \partial_\mu \alpha) - \frac{\tau_c f_0 \tilde{f}_0}{u.p} q \beta E^\nu p_\nu \\
&= \frac{\tau_c f_0 \tilde{f}_0}{u.p} (\beta p^\phi p^\phi r u_r - \beta p^\eta p^\eta \tau u_\tau + (u.p) p^\mu \partial_\mu \beta - p^\mu \partial_\mu \alpha) - \frac{\tau_c f_0 \tilde{f}_0}{u.p} q \beta E^\nu p_\nu \\
&\quad + \frac{\tau_c f_0 \tilde{f}_0}{u.p} (\beta p^\tau p^\tau \partial_\tau u_r + \beta p^r p^r \partial_r u_r + \beta p^\phi p^\tau \partial_\phi u_r) + \frac{\tau_c f_0 \tilde{f}_0}{u.p} (\beta p^\tau p^\tau \partial_\tau u_r + \beta p^r p^r \partial_r u_r + \beta p^\phi p^\tau \partial_\phi u_r) \\
&= \frac{\tau_c f_0 \tilde{f}_0}{u.p} \left(\beta \left(\frac{p_T \sin(\varphi - \phi)}{r} \right)^2 r u_r - \beta \left(\frac{m_T \sinh(y - \eta)}{\tau} \right)^2 \tau u_\tau + (u.p) p^\mu \partial_\mu \beta - p^\mu \partial_\mu \alpha \right) \\
&\quad - \frac{\tau_c f_0 \tilde{f}_0}{u.p} q \beta E^\nu p_\nu + \frac{\tau_c f_0 \tilde{f}_0}{u.p} \left(\beta m_T \cosh(y - \eta) p_T \cos(\varphi - \phi) \frac{(u^r)^2}{r u^\tau} - \beta (p_T \cos(\varphi - \phi))^2 \frac{u^r}{r} \right) \\
&\quad + \frac{\tau_c f_0 \tilde{f}_0}{u.p} \beta \frac{p_T \sin(\varphi - \phi)}{r} p_T \cos(\varphi - \phi) u_0 \frac{2r}{R} \sum n u_n \sin n [\phi - \psi_n] \\
&\quad + \frac{\tau_c f_0 \tilde{f}_0}{u.p} \left(-\beta (m_T \cosh(y - \eta))^2 \frac{(u^r)^3}{r (u^\tau)^2} + \beta m_T \cosh(y - \eta) p_T \cos(\varphi - \phi) \frac{(u^r)^2}{r u^\tau} \right) \\
&\quad - \frac{\tau_c f_0 \tilde{f}_0}{u.p} \beta \frac{p_T \sin(\varphi - \phi)}{r} m_T \cosh(y - \eta) \frac{u^r}{u^\tau} u_0 \frac{2r}{R} \sum n u_n \sin n [\phi - \psi_n], \\
\delta f &= \frac{\tau_c f_0 \tilde{f}_0}{u.p} \beta \left(\frac{u_r}{r} + \frac{\sin(\varphi - \phi) \cos(\varphi - \phi)}{r} u_0 \frac{2r}{R} \sum u_n n \sin n [\phi - \psi_n] \right) p_T^2 - \frac{\tau_c f_0 \tilde{f}_0}{u.p} q \beta E^\nu p_\nu \\
&\quad + \frac{\tau_c f_0 \tilde{f}_0}{u.p} \beta \left(2 \cosh(y - \eta) \cos(\varphi - \phi) \frac{(u^r)^2}{r u^\tau} - \cosh(y - \eta) \sin(\varphi - \phi) \frac{u^r}{r u^\tau} u_0 \frac{2r}{R} \sum u_n n \sin n [\phi - \psi_n] \right) m_T p_T \\
&\quad - \frac{\tau_c f_0 \tilde{f}_0}{u.p} \beta \left(\sinh^2(y - \eta) \frac{u_\tau}{\tau} + \cosh^2(y - \eta) \frac{(u^r)^3}{r (u^\tau)^2} \right) m_T^2 + \frac{\tau_c f_0 \tilde{f}_0}{u.p} ((u.p) p^\mu \partial_\mu \beta - p^\mu \partial_\mu \alpha),
\end{aligned}$$

where $\beta = \frac{1}{T}$ and $\alpha = \frac{\mu}{T}$ with $\Gamma_{\eta\eta}^\tau = \tau$ along with $\Gamma_{\phi\phi}^r = -r$. The contribution due to the electric field $E \cdot p$ in the above equation, when expanded, takes the following form

$$\begin{aligned}
\delta f &= -\frac{\tau_c f_0 \tilde{f}_0}{u.p} q \beta E \cdot p, \\
\delta f &= -\frac{\tau_c f_0 \tilde{f}_0}{u.p} q \beta (E^\tau p^\tau - \tau^2 E^\eta p^\eta - E^r p^r - r^2 E^\phi p^\phi).
\end{aligned}$$

1. Co-ordinate transformation of Electric four vector

The electric field components in Milne-coordinates $(E^\tau, E^\eta, E^r, E^\phi)$ are connected to the Cartesian components (E^t, E^x, E^y, E^z) through the following transformation

$$\begin{bmatrix} E^\tau \\ E^r \\ E^\phi \\ E^\eta \end{bmatrix} = \begin{bmatrix} \text{Cosh}[\eta] & 0 & 0 & -\text{Sinh}[\eta] \\ 0 & \text{Cos}[\phi] & \text{Sin}[\phi] & 0 \\ 0 & -\frac{\text{Sin}[\phi]}{r} & \frac{\text{Cos}[\phi]}{r} & 0 \\ -\frac{\text{Sinh}[\eta]}{\tau} & 0 & 0 & \frac{\text{Cosh}[\eta]}{\tau} \end{bmatrix} \begin{bmatrix} E^t \\ E^x \\ E^y \\ E^z \end{bmatrix}.$$

We also note $E \cdot u = 0$ and this gives rise to :

$$E^t = \frac{E^z \text{Sinh}\eta}{\text{cosh}\eta} + \frac{(\text{cos}\phi E^x + \text{sin}\phi E^y)u^r}{\text{cosh}\eta\tau},$$

$$E^\eta = \frac{E^z}{\tau \text{Cosh}\eta} - \frac{\text{tanh}\eta E^r u^r}{\tau u^\tau}.$$

As mentioned in the main text we use four different configuration of transverse electric fields, they are parameterised as :

$$eE_x = \frac{\mathcal{B}Z\alpha_{em}(x-x_0)\text{Cosh}[\eta-\eta_0]}{((x-x_0)^2 + (y-y_0)^2 + (\tau\text{Sinh}[\eta-\eta_0])^2)^{3/2}},$$

$$eE_y = \frac{\mathcal{A}Z\alpha_{em}(y-y_0)\text{Cosh}[\eta-\eta_0]}{((x-x_0)^2 + (y-y_0)^2 + (\tau\text{Sinh}[\eta-\eta_0])^2)^{3/2}},$$

$$eE_z = 0,$$

where Z is the atomic number (for our case we choose $Z=82$), $\alpha_{em}=\frac{1}{137}$, \mathcal{A} and \mathcal{B} are the modulation factors which controls the spatial configuration of the field in the transverse plane, and α is the fine structure constant. We get the first 3 configurations in Fig.(2) by choosing (i) $\mathcal{A}=\mathcal{B}=10$ for **config-1**, (ii) $\mathcal{A}=20$, $\mathcal{B}=1$ for **config-2** (iii) $\mathcal{A}=1$, $\mathcal{B}=20$ for **config-3**, and $qE_x = qE_y = m_\pi^2$ for **config-4**.

-
- [1] K. G. Wilson, Confinement of quarks, *Phys. Rev. D* **10**, 2445 (1974).
- [2] F. Karsch, E. Laermann, and A. Peikert, The pressure in 2, 2+1 and 3 flavour QCD, *Physics Letters B* **478**, 447 (2000).
- [3] P. Romatschke and U. Romatschke, Viscosity information from relativistic nuclear collisions: How perfect is the fluid observed at rhic?, *Phys. Rev. Lett.* **99**, 172301 (2007).
- [4] H. Song and U. Heinz, Causal viscous hydrodynamics in 2 + 1 dimensions for relativistic heavy-ion collisions, *Phys. Rev. C* **77**, 064901 (2008).
- [5] P. K. Kovtun, D. T. Son, and A. O. Starinets, Viscosity in strongly interacting quantum field theories from black hole physics, *Phys. Rev. Lett.* **94**, 111601 (2005).
- [6] D. E. Kharzeev, L. D. McLerran, and H. J. Warringa, The Effects of topological charge change in heavy ion collisions: 'Event by event P and CP violation', *Nucl. Phys. A* **803**, 227 (2008), arXiv:0711.0950 [hep-ph].
- [7] V. Skokov, A. Y. Illarionov, and V. Toneev, Estimate of the magnetic field strength in heavy-ion collisions, *Int. J. Mod. Phys. A* **24**, 5925 (2009), arXiv:0907.1396 [nucl-th].
- [8] K. Tuchin, Erratum: Synchrotron radiation by fast fermions in heavy-ion collisions [phys. rev. c 82, 034904 (2010)], *Phys. Rev. C* **83**, 039903 (2011).
- [9] V. Voronyuk, V. D. Toneev, W. Cassing, E. L. Bratkovskaya, V. P. Konchakovski, and S. A. Voloshin, Electromagnetic field evolution in relativistic heavy-ion collisions, *Phys. Rev. C* **83**, 054911 (2011).
- [10] W.-T. Deng and X.-G. Huang, Event-by-event generation of electromagnetic fields in heavy-ion collisions, *Phys. Rev. C* **85**, 044907 (2012).
- [11] K. Tuchin, Particle production in strong electromagnetic fields in relativistic heavy-ion collisions, *Adv. High Energy Phys.* **2013**, 490495 (2013), arXiv:1301.0099 [hep-ph].
- [12] L. McLerran and V. Skokov, Comments About the Electromagnetic Field in Heavy-Ion Collisions, *Nucl. Phys. A* **929**, 184 (2014), arXiv:1305.0774 [hep-ph].
- [13] W. Israel and J. Stewart, Transient relativistic thermodynamics and kinetic theory, *Annals of Physics* **118**, 341 (1979).
- [14] G. S. Denicol, X.-G. Huang, E. Molnár, G. M. Monteiro, H. Niemi, J. Noronha, D. H. Rischke, and Q. Wang, Nonresistive dissipative magnetohydrodynamics from the Boltzmann equation in the 14-moment approximation, *Phys. Rev. D* **98**, 076009 (2018), arXiv:1804.05210 [nucl-th].
- [15] G. S. Denicol, E. Molnár, H. Niemi, and D. H. Rischke, Resistive dissipative magnetohydrodynamics from the Boltzmann-Vlasov equation, *Phys. Rev. D* **99**, 056017 (2019), arXiv:1902.01699 [nucl-th].
- [16] A. K. Panda, A. Dash, R. Biswas, and V. Roy, Relativistic non-resistive viscous magnetohydrodynamics from the

- kinetic theory: a relaxation time approach, *JHEP* **03**, 216, [arXiv:2011.01606 \[nucl-th\]](#).
- [17] A. K. Panda, A. Dash, R. Biswas, and V. Roy, Relativistic resistive dissipative magnetohydrodynamics from the relaxation time approximation, *Phys. Rev. D* **104**, 054004 (2021), [arXiv:2104.12179 \[nucl-th\]](#).
- [18] A. K. Panda and V. Roy, Wave Phenomena In General Relativistic Magnetohydrodynamics (2022), [arXiv:2205.03107 \[gr-qc\]](#).
- [19] E. R. Most and J. Noronha, Dissipative magnetohydrodynamics for nonresistive relativistic plasmas: An implicit second-order flux-conservative formulation with stiff relaxation, *Phys. Rev. D* **104**, 103028 (2021), [arXiv:2109.02796 \[astro-ph.HE\]](#).
- [20] U. Gürsoy, D. Kharzeev, and K. Rajagopal, Magnetohydrodynamics, charged currents, and directed flow in heavy ion collisions, *Phys. Rev. C* **89**, 054905 (2014).
- [21] U. Gürsoy, D. Kharzeev, E. Marcus, K. Rajagopal, and C. Shen, Charge-dependent flow induced by magnetic and electric fields in heavy ion collisions, *Phys. Rev. C* **98**, 055201 (2018).
- [22] K. Nakamura, T. Miyoshi, C. Nonaka, and H. R. Takahashi, Relativistic resistive magneto-hydrodynamics code for high-energy heavy-ion collisions (2022), [arXiv:2211.02310 \[nucl-th\]](#).
- [23] G. Inghirami, L. Del Zanna, A. Beraudo, M. H. Moghadam, F. Becattini, and M. Bleicher, Numerical magnetohydrodynamics for relativistic nuclear collisions, *Eur. Phys. J. C* **76**, 659 (2016), [arXiv:1609.03042 \[hep-ph\]](#).
- [24] E. Schnedermann, J. Sollfrank, and U. W. Heinz, Thermal phenomenology of hadrons from 200-A/GeV S+S collisions, *Phys. Rev. C* **48**, 2462 (1993), [arXiv:nucl-th/9307020](#).
- [25] K. Fukushima, D. E. Kharzeev, and H. J. Warringa, Chiral magnetic effect, *Phys. Rev. D* **78**, 074033 (2008).
- [26] Y. Burnier, D. E. Kharzeev, J. Liao, and H.-U. Yee, Chiral magnetic wave at finite baryon density and the electric quadrupole moment of the quark-gluon plasma, *Phys. Rev. Lett.* **107**, 052303 (2011).
- [27] D. E. Kharzeev and H.-U. Yee, Chiral magnetic wave, *Phys. Rev. D* **83**, 085007 (2011).
- [28] J.-J. Zhang, X.-L. Sheng, S. Pu, J.-N. Chen, G.-L. Peng, J.-G. Wang, and Q. Wang, Charge-dependent directed flows in heavy-ion collisions by Boltzmann-Maxwell equations (2022), [arXiv:2201.06171 \[hep-ph\]](#).
- [29] G. Inghirami, M. Mace, Y. Hirono, L. Del Zanna, D. E. Kharzeev, and M. Bleicher, Magnetic fields in heavy ion collisions: flow and charge transport (2020), [arXiv:1908.07605 \[hep-ph\]](#).
- [30] V. Roy, S. Pu, L. Rezzolla, and D. H. Rischke, Effect of intense magnetic fields on reduced-MHD evolution in $\sqrt{s_{NN}} = 200$ GeV Au+Au collisions, *Phys. Rev. C* **96**, 054909 (2017), [arXiv:1706.05326 \[nucl-th\]](#).
- [31] T. Gezhagn and A. K. Chaudhury, Electromagnetic Field Evolution in Relativistic Heavy Ion Collision and Its Effect on Flow of Particles, *Front. in Phys.* **9**, 791108 (2022), [arXiv:2107.01467 \[nucl-th\]](#).
- [32] X.-G. Huang, Electromagnetic fields and anomalous transports in heavy-ion collisions — A pedagogical review, *Rept. Prog. Phys.* **79**, 076302 (2016), [arXiv:1509.04073 \[nucl-th\]](#).
- [33] F. Cooper and G. Frye, Single-particle distribution in the hydrodynamic and statistical thermodynamic models of multiparticle production, *Phys. Rev. D* **10**, 186 (1974).
- [34] S. K. Das *et al.*, Dynamics of Hot QCD Matter – Current Status and Developments (2022) [arXiv:2208.13440 \[nucl-th\]](#).
- [35] B. Abelev *et al.* (ALICE), Centrality dependence of π , K, p production in Pb-Pb collisions at $\sqrt{s_{NN}} = 2.76$ TeV, *Phys. Rev. C* **88**, 044910 (2013), [arXiv:1303.0737 \[hep-ex\]](#).
- [36] V. Roy and A. K. Chaudhuri, Lattice based equation of state and transverse momentum spectra of identified particles in ideal and viscous hydrodynamics, *DAE Symp. Nucl. Phys.* **55**, 624 (2010), [arXiv:1003.1195 \[nucl-th\]](#).
- [37] J. Noronha-Hostler, J. Noronha, and F. Grassi, Bulk viscosity-driven suppression of shear viscosity effects on the flow harmonics at energies available at the bnl relativistic heavy ion collider, *Phys. Rev. C* **90**, 034907 (2014).
- [38] G. S. Denicol, T. Kodama, and T. Koide, The effect of shear and bulk viscosities on elliptic flow, *J. Phys. G* **37**, 094040 (2010), [arXiv:1002.2394 \[nucl-th\]](#).